FULL PAPER

Alcohol as a Processing Solvent of Polymeric Semiconductors to Fabricate Environmentally Benign and High Performance Polymer Field Effect Transistors

Kwang Hee Cheon, Hyungju Ahn, Jangwhan Cho, Hui-Jun Yun, Byung Tack Lim, Dong Jin Yun, Han-Koo Lee, Soon-Ki Kwon, Yun-Hi Kim, and Dae Sung Chung**

Here, a novel strategy is reported to develop polymer field effect transistors using ethanol, propanol, and butanol—the most environmentally benign solvent except water—as processing solvents. From such environmentally benign processes, for the first time high-mobility (>1 $cm^2 V^{-1} s^{-1}$) polymer field effect transistors are demonstrated. These mobility values realized from "really green solvents" exceed those of conventional hydrogenated amorphous silicon semiconductors. To achieve this 1) stable sub-microparticles of conjugated polymers dispersed in alcohols are fabricated, 2) an aldehyde-assisted surface tension-depression methodology is developed to successfully form thin films from alcohol, and 3) the structural information of alcohol-dispersed sub-microparticles of semiconducting polymers is carefully characterized.

1. Introduction

Solution-processable polymeric semiconductors have been of great interest because of their potential in several industrially relevant technologies, including field effect transistors (FETs),[1–3] photovoltaic cells,[4,5] photodetectors,[6] and memory devices.[7] They have significant advantages over inorganic semiconductors and small molecular semiconductors because they can be used in the ultra low-cost fabrication of large-area devices via high-throughput printing, owing to their robust, stable, and reliable electrical/physical characteristics.[8] Moreover, recent studies on designing novel molecular structures introduced strong donor-acceptor copolymerization strategies, which have helped realize unprecedented high mobilities exceeding 10 $cm^2 V^{-1} s^{-1}$,[1–3] compatible with a realistic minimum requirement for driving FETs of commercial organic light emitting diodes.[9]

Until now, almost all research efforts in polymer FETs (PFETs) have focused on improving the mobility value, because it remained less than 1 $cm^2 V^{-1} s^{-1}$ for long time, and only very recently has this value been overcome.[10] As a consequence, unfortunately there has been little research on improving processing solvents of such PFETs, and thus, good film-forming but very toxic halogenated solvents such as chloroform and chlorobenzene have been widely used.[11] These toxic solvents unnecessarily increase environmental costs as they require undesirable procedures for production, use, and waste removal.[12] Therefore, the ability to process polymeric semiconductors from environmentally benign solvents such as ethanol, or even water, can make them much stronger candidates for industrial electronic applications at a lower cost.

Accordingly, several methodologies have been tried that can enable the processing of polymeric semiconductors in "greener" solvents to realize environmentally benign PFETs.[11,13–17] For example, in 2009, Lu and co-workers reported the synthesis of an ethanol-soluble polythiophene derivative with oxetane substitution in the side chain with a mobility of $\approx 10^{-3}$ $cm^2 V^{-1} s^{-1}$ in a PFET,[16] which can be viewed as a target value for the highest mobility from water or ethanol-processed PFETs. Apart from ethanol and water, a few studies tried relatively greener solvents such as p-xylene and tetrahydronaphthalene to process polymeric semiconductors, resulting in high mobility of >1 $cm^2 V^{-1} s^{-1}$.[18,19] However, those organic solvents can still

K. H. Cheon, J. Cho, B. T. Lim, Prof. D. S. Chung
School of Chemical Engineering and Material Science
Chung-Ang University
Seoul 156-756, South Korea
E-mail: dchung@cau.ac.kr
Dr. H. Ahn, Dr. H.-K. Lee
Pohang Accelerator Laboratory
San 31 Hyojadong, Namgu, Pohang, Kyung-Buk 790-784, South Korea
H.-J. Yun, Prof. S.-K. Kwon
School of Materials Science and Engineering and ERI
Gyeongsang National University
Jinju 660-701, South Korea
Dr. D. J. Yun
Analytical Science Laboratory Samsung Advanced Institute of Technology
Suwon 443-806, South Korea
Prof. Y.-H. Kim
Department of Chemistry and ERI
Gyeongsang National University
Jinju 660-701, South Korea
E-mail: ykim@gnu.ac.kr

DOI: 10.1002/adfm.201500877

be categorized as harmful solvents according to their materials safety data sheets (MSDS).[20] or other widely known report,[21] as summarized in Tables S1–S5 of the Supporting Information. Therefore, it is still highly desirable to develop really "green" processes without compromising the high-mobility nature of polymeric semiconductors.

The work presented in this paper starts from the question: "Do we really need to perfectly dissolve polymeric semiconductors to fabricate high-performance PFETs?" We show that polymeric semiconductors that are simply dispersed (not dissolved) in low-molecular-weight alcohol—ethanol, propanol, and butanol—in a sub-micrometer sizes can be a reasonably good processing solution for fabricating high-performance PFETs with mobilities exceeding 1 $cm^2 V^{-1} s^{-1}$. Actually, such polymer colloids techniques have been widely applied in the field of adhesive, paint-, biomedial, and conducting polymer industries.[22–25] Interest in polymer colloids—usually defined as a dispersion of submicron polymer particles in a liquid medium—was also spurred by environmental considerations to switch from solvent-based to water-borne systems. Therefore, our approach can be viewed as a new polymer colloids technique for semiconducting polymer, considering there have been no efforts to fabricate semiconducting polymer-based colloids to be used as high performance PFETs. To this end, random copolymers consisting of two slightly different but highly conductive repeating units, namely, diketopyrrolopyrrole-selenophene-vinylene-selenophene (DPP-SVS) and DPP-thienothiophene (DPP-TT) with relatively high structural randomness was employed,[18,19] enabling better dispersibility in various alcohols. To enhance the film-forming characteristics of alcohol-based polymer solutions, which inherently suffer from high surface tension, a small amount (5 vol%) of aldehyde was added to decrease the surface tension of the alcohols, resulting in a fine film.[26] Various X-ray tools, including area-selective X-ray photoelectron spectroscopy (XPS) and grazing incident X-ray diffraction (GIXD), were employed to prove that alcohol-processed thin films of polymeric semiconductors consisting of micrometer-sized clusters still reveal ordered crystalline nature. We demonstrate that this strategy works with various device geometries with channel lengths varying from several micrometers to several hundreds of micrometers, and also with low-voltage device architecture.

2. Results and Discussion

Among various comonomer ratios between DPP-TT and DPP-SVS, we chose P-DPP-TT(7)-SVS(3) (in short, P1) where the contents of the DPP-SVS unit is ≈30%,[27] because it enabled the fastest dispersion in alcohols The dispersion time of P1 is compared to other copolymers with different comonomer ratios in Figure S1, Supporting Information. Because we maintained the molecular weights of all the copolymers within the similar range (Table S7, Supporting Information), we might attribute the shortest dispersion time of P1 to its relatively higher segmental randomness within the polymer chains and also to relatively lower contents of SVS moiety which leads to lower solubility of copolymer. P1 (chemical structure in **Figure 1**a) could be dispersed in low-molecular-weight alcohols, including ethanol, propanol, butanol, hexanol, and octanol. Among these, ethanol, propanol, and butanol revealed relatively "greener" characteristics according to their MSDSs or other previous reports, and therefore, were selected as target solvents in this

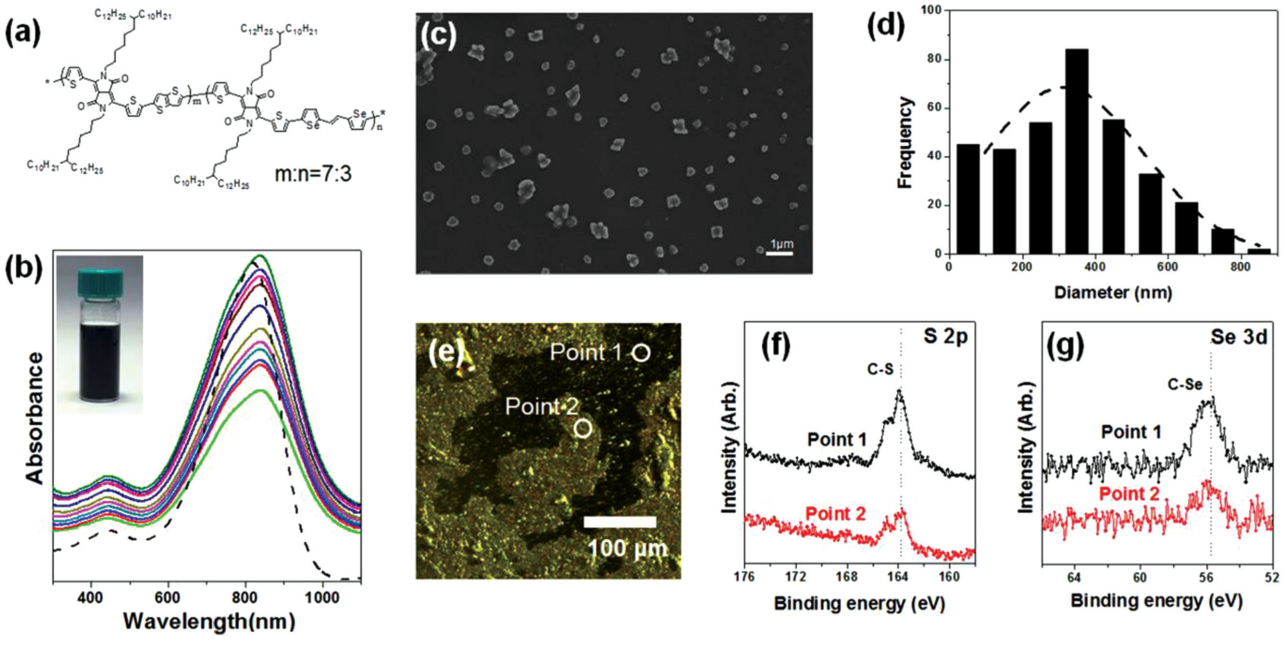

Figure 1. a) Chemical structure of P1 used in this communication as an alcohol-dispersed polymeric semiconductor. b) UV–vis absorption spectra of P1 dispersed in butanol as a function of sonication time with 5 min of interval. Longer sonication time yielded higher absorption intensity of P1. The dashed line corresponds to the absorption spectra of P1 dissolved in chloroform. (Inset: the actual digital image of P1 dispersed in butanol.) c) The SEM image of distributed sub-microparticles of P1 and d) the result of size distribution analysis. e) The optical microscopy image of the fabricated blend film. f–g) The area selective XPS spectra corresponding to f) C–S bonding in S 2p core level structure and g) C–Se bonding in Se 3d core level structures.

study (Tables S1–S5, Supporting Information).[20,21] In addition, these small alcohols are known to merely contaminate water in the environment, which can be an important benefit from the industrial point of view.[28] Figure 1b shows time-dependent UV–vis absorption spectra of P1 dispersed in butanol (0.1 mg mL^{-1}, sonicated at 40 °C) taken at 5 min intervals. After approximately 35 min, the absorption spectra reached steady-state, and no further fine dispersion could be observed. The dispersion time, defined as the consumed time to reach at the steady-state absorption spectra, of random copolymer was much shorter than pristine, regular polymers as summarized in Figure S1 in the Supporting Information. This can be partially understood by increased segmental randomness of the random copolymer compared to regular polymers.[19] The absorption maximum of P1 dispersed in butanol was observed at ≈838 nm, red-shifted 22 nm from that of the chloroform solution, which is regarded as a perfectly dissolved solution. In ethanol, P1 showed similar absorption behavior (summarized in Figure S2 of the Supporting Information), implying that microparticles of P1 are physically dispersed in alcohols, without damaging the polymer structure via oxidation. To characterize the polymers dispersed in butanol, we used scanning electron microscopy (SEM) on the polymer microparticles cast on the Si wafer and the resulting image is depicted in Figure 1c. Although the size distribution (Figure 1d) is not narrow, one can see the presence of the well-dispersed sub-microparticles with average size ≈300 nm. Because the aim of this work is demonstrating high performance PFET, we did not try to further enhance the size distribution of the sub-microparticles. To make thin films, P1-containing alcohol solutions were spin- or drop-cast on precleaned Si/SiO_2 substrates without any buffer layers. Alcohol itself has an unfavorable film-forming nature due to its high surface tension, and therefore, pure butanol or ethanol cannot result in reasonably good P1 films. To decrease the surface tension and to enhance the film-forming nature of alcohols, a small amount of butyraldehyde (5%), which can still be categorized as a "green" solvent, was added to P1-dispersed alcohol solutions. As summarized in Figure S3 of the Supporting Information, increasing amount of aldehyde leads to decrease in surface tension of the butanol solution, presumably due to smaller intermolecular interaction force of aldehyde molecules rather than alcohol molecules. Almost 5% of surface tension decrease of butanol is observed by adding only 5% of butyraldehyde. Actually, the contact angle of butyraldehyde droplet on the Si-wafer substrate is apparently smaller than alcohol droplet on the same substrate as shown in Figure S4 of the Supporting Information. More importantly, wettability of butanol was significantly enhanced by addition of aldehyde especially at the elevated temperature of 80 °C. (Figure S5, Supporting Information) In addition to the aldehyde strategy, to further enhance the thin-film characteristics of alcohol-processed P1, polyvinylidene fluoride (PVDF) was also added to the alcohol solution, which was expected to play the role of a matrix polymer. However, we noted that the addition of PVDF was not very necessary for fine film formation and FET performance; even without PVDF, we could still observe good FET performance with only slightly lower mobility. Figure 1e shows the optical microscope (OM) images of the resulting films and Figure 1f–g shows their area-selective XPS analysis data. From OM images, it is clear that the thin films are composed of two distinct phases, which appear as dark and bright colors, respectively. As confirmed by the cross-sectional height profile, (not shown) the bright and dark phases correspond to higher and lower altitudes, respectively. To elucidate the chemical composition of each laterally separated phase, we conducted area-selective XPS analysis on points 1 (dark) and 2 (bright), as depicted in Figure 1f,g. Relatively pronounced signals from C–S bonding in S 2p core level structure (2.68 at%) and C–Se bonding in Se 3d core level structure (0.33 at%) bonds were observed at point 1 (dark), while much weaker signals of 0.84 and 0.08 at%, respectively, were observed at point 2 (bright). Therefore, it is plausible that the dark phase (point 1) corresponds to the clusters of P1 sub-microparticles, and the bright phase (point 2) corresponds to amorphous PVDF. Some minor C–S or C–Se signals observed in the bright phase may indicate the existence of very small P1 clusters. Overall, these results indicate that the P1 film cast from alcohol is simply viewed as an aggregation of P1 sub-microparticles in conjunction with PVDF. Then, if the P1 sub-microparticles retain a well-aligned semicrystalline nature, we can expect high-performance PFETs, even though they were processed from alcohols.

GIXD analysis was performed to investigate the crystalline nature and molecular orientation of P1 films. P1 films cast from butanol, ethanol, and chloroform are prepared by thermal annealing at 200 °C, and their 2D-GIXD images, in-plane and out-of-plane intensity profiles are shown in **Figure 2**a–e. In the 2D GIXD patterns, q_{xy} and q_z represents the in-plane and out-of-plane components of the scattering vector q, respectively; these components are normal to the plane of incidence and the sample surface plane, respectively. In both cases of butanol- and ethanol-based films, the 2D GIXD pattern of P1 films exhibited out-of-plane (n00) diffraction peaks, up to fourth-order diffraction, with additional multiple-diffracted intensity observed in in-plane intensity profiles. The (100) layer distance of each P1 film, i.e., the d-spacing (=$2\pi/q^*$), was derived from the in-plane and out-of-plane intensity profiles. The (100) layer distance of butanol- and ethanol-based films was 30.0 and 29.0 Å, respectively. Additionally, a relative weak peak at q_{xy} = ≈1.74 and q_z = ≈1.73 $Å^{-1}$ was observed in the in-plane and out-of-plane intensity profiles, respectively. These can be attributed to the formation of intermolecular π–π stacking with distance ≈3.6 Å. Especially, the (100) and (010) diffraction attributing to π–π staking peaks were observed at both out-of-plane and in-plane intensity profiles, implying the presence of a mixture of face-on and edge-on orientation. In case of chloroform-based P1 film, the 2D GIXD images and out-of-plane intensity profiles present well-defined diffraction peaks up to (500) diffraction along the out-of-plane direction. Moreover, the distinct (010) diffraction peak was only observed in the in-plane intensity profiles. These results indicate that chloroform-based P1 films have a strong preference for the edge-on molecular orientation. The (100) layer and π-staking distance of chloroform-based P1 film were 30.9 and 3.6 Å, respectively.

The information about the size of crystalline grains is contained in the width of the diffraction peaks. The size of crystalline grain can be simply calculated by the Scherrer equation. However, this method is only valid for the finite size of the crystalline assemblies.[29] In the organic semiconductor

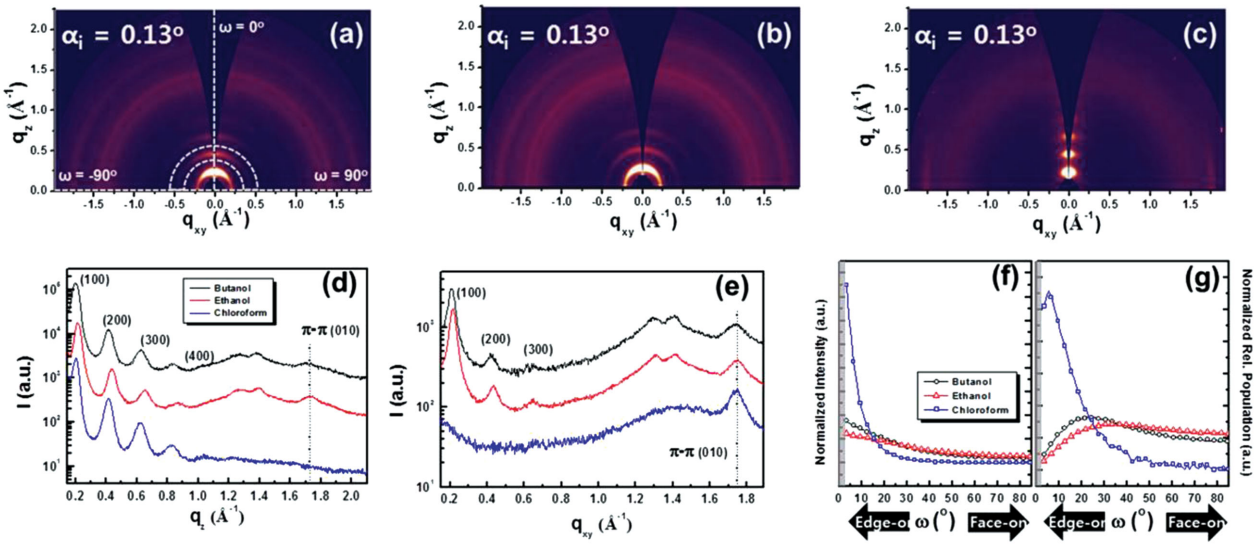

Figure 2. GIXD images of thin films obtained from a) butanol, b) ethanol, and c) chloroform solution and their corresponding extracted profiles along with d) out-of-plane direction and e) in-plane direction. f) The pole figures for each film normalized by (200) scattered intensity. g) The pole figures multiplied by a factor of sin ω to reflect geometrical effects. The gray-shade regions in (f–g) indicate inaccessible ω range. All the films were thermally (200 °C) treated for 20 min.

system, the width of first order diffraction peak cannot directly provide a grain size, due to the cumulative disorder effect (or paracrystalline disorder effect).[30] With considering paracrystalline disorder effect, the paracrystalline distortion parameter (g) and true paracrystal size ($\overline{L}_c$) nomal to the (n00) plane were calculated from the slope ($=g^2\pi^2/d$; d is the domain spacing) and intercept ($=1/\overline{L}_c$) of the δb-m^2 plot, where δb is the integral width of the diffraction peaks calculated from $\delta b = 1/L_c$ (L_c: coherence length) and m is the order of diffraction. The δb-m^2 plot of P1 films extracted from out-of-plane intensity profiles are presented in Figure S6, Supporting Information. The calculated paracrystalline distortion parameter (g) values of P1 films were 2.8%, 2.4%, and 3.3% for butanol-, ethanol-, and chloroform-based films, respectively. The total crystallographic parameters of P1 films are presented in Table S8 of the Supporting Information. Especially, the true paracrystalline size (L_c) of P1 films was 140.8, 147.2, and 169.49 Å for butanol-, ethanol-, and chloroform-based films, respectively. These results imply that P1 molecules dispersed in alcohol experienced much shorter crystallization time compared to the case of chloroform, resulting in relatively shorter crystalline size.

To further elucidate the crystalline orientation of P1 films, we conducted pole figure analyses as presented in Figure 2f–g. Pole figure analyses enable to study the orientational distribution of the diffraction peaks as a function of all possible crystalline orientation.[29] The pole figures presented in Figure 2f were normalized by (200) scattered intensity for each film, in order to facilitate comparison. For the pole figure analysis, we analyzed the distribution of (200) orientations to avoid the surface scattering effects resulting from the substrate. Due to the geometry of the GIXD experiment and the curved surface of the Ewald sphere, the detector angle is not exactly matched with polar angle (ω). At $q \approx 0.42$ Å^{-1} ((200) peak position), the zero angle of detector plane corresponds to $\omega \approx 2.15°$, so we cannot obtain the intensity information for the orientation $\omega < 2.15°$. The inaccessible ω range is designated by gray-shade region in Figure 2f–g. The pole figure shows that all the P1 films adopt a preferential edge-on orientation. Especially, the most of crystallines in chlroform-based film are preferentially oriented within a polar angle of 16°, while crystallines in butanol- and ethanol-based P1 films are widely distributed within a polar angle of 47° and 58°, respectively. To correct for geometrical effects, the intensity profile in the pole figure must be multiplied by a factor of sin ω as shown in Figure 2g. Here, relative population profile was normalized by relative degree of crystallinity (rDoC) for the easy comparison between samples. The rDoC of P1 sample was calculated by integration of relative population distribution with considering the factor of X-ray exposure time, beam foot-print, thickness of sample, and polymer volume fraction.[31] The calculated rDoC values were 1.0, 0.98, and 5.90 for butanol-, ethanol-, and chloroform-based films, respectively. The large difference of rDoC between chloroform- and alcohol-based films might be induced by greatly different processing conditions for crystalline formation. In Figure 2g, the chloroform-based film exhibited significantly large edge-on population with a maximum at about $\omega = 6°$. The butanol-based film showed broad orientation population profiles with a maximum at about $\omega \approx 25°$, but the edge-on orientation ($\omega < 45°$) is still dominant. In case of the ethanol based P1 film, the maximum population was observed at about $\omega = 35°$ with a random distribution, which is reflected by the nearly constant population at $\omega = 40°$–$90°$.

Consequently, these results imply that the alcohol-processed films have less edge-on orientation of the crystalline domain compared to chloroform-processed films. In conclusion, the structural analyses indicate that chloroform enables the well-defined edge-on orientation, and butanol enables a more distributed crystallite orientation. In the case of ethanol, the

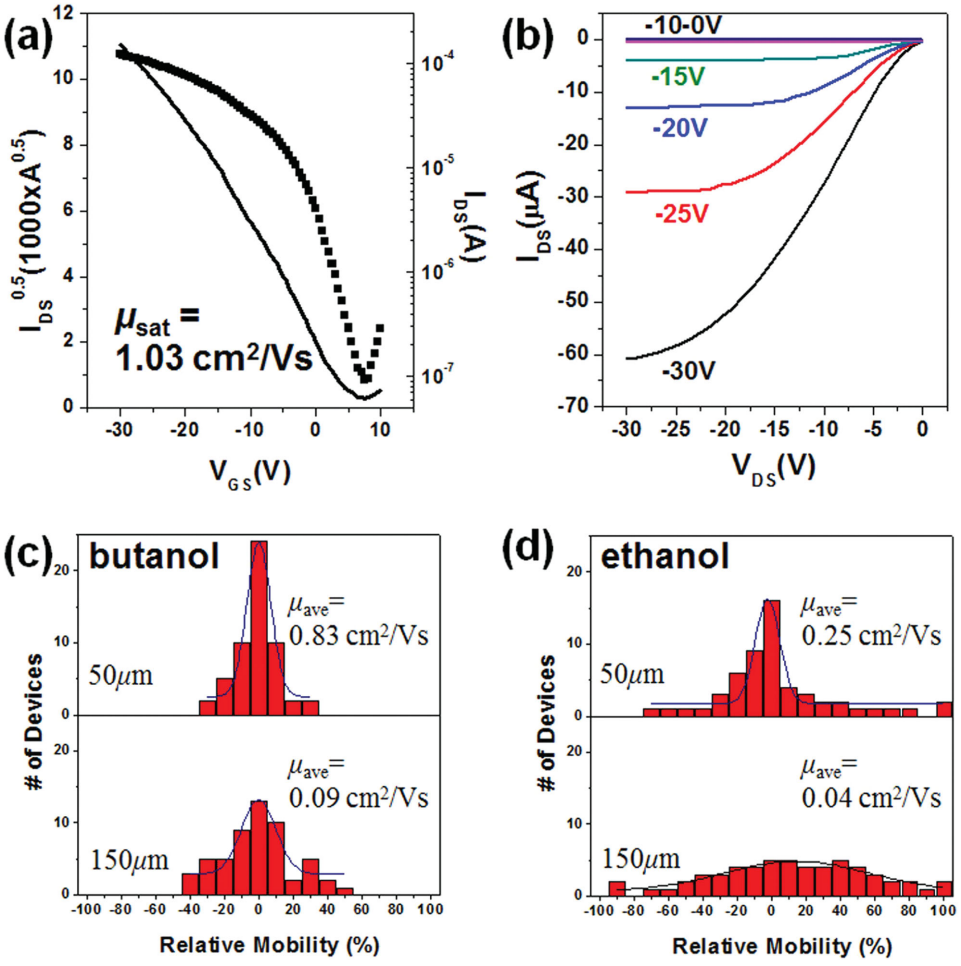

Figure 3. The representative a) transfer and b) output characteristics of P1 PFET fabricated from butanol. The statistical distribution of measured mobility values obtained from c) butanol-based PFET and d) ethanol-based PFET. In each figure, upper and lower panel corresponds to short channel (50 μm) and long channel (150 μm) device.

resulting P1 film showed the worst edge on orientation, possibly due to its having the worst dispersibility. However, these results also imply that alcohol-processed films still maintain some degree of edge-on crystalline orientation of crystalline domain, which can lead to efficient charge transport.

To test the FET performances of alcohol-processed P1, we fabricated PFETs with various device geometries. From conventional bottom-gate/bottom-electrode geometries with relatively short channel lengths (3–50 μm), we were able to obtain the highest FET mobility, up to 1.03 $cm^2\ V^{-1}\ s^{-1}$, under a saturation regime. The representative transfer and output characteristics are summarized in **Figure 3**a,b, respectively. Interestingly, in the case of the bottom-gate/top-electrode geometries with relatively longer channel lengths (100–150 μm), we obtained slightly lower FET performances, with mobility ≈0.1 $cm^2\ V^{-1}\ s^{-1}$, although this device configuration allows for a better charge injection environment. In Figure 3 and Figure S7, Supporting Information, we fully summarize the measured mobility values from PFETs processed from various channel lengths. Clearly, one can see that the shorter channel length enables higher mobility, as well as narrower device-to-device deviations. This result can be related to the size of aggregated clusters (30–100 μm) of P1 sub-microparticles cast from alcohols. When the channel length exceeded the average size of the aggregated clusters, there was slight but clear evidence of mobility decreases, as shown in Figure 3 (and also in Figure S7, Supporting Information). In a similar context, we can expect a narrower distribution of mobility values in the case of short channel devices, because all of the clusters larger than 10 μm can contribute to electrical current, while only extremely large clusters (>100 μm) can contribute to electrical current in the case of long channel devices. The spin coating speed also greatly affected the PFET performances due to different sizes of aggregated P1 clusters. As Figure S8 in the Supporting Information presents, the higher spin-coating speeds in rpm always yielded lower sizes of aggregated clusters, apparently smaller than the channel length, presumably due to shorter time for film formation. Therefore, we could observe reasonably high performance only when we used low spin-coating speed of ≈500 rpm or drop-casting techniques. We also address that the above-mentioned morphological factor was much more decisive on PFET performances rather than the comonomer

ratios of copolymers (between DPP-TT and DPP-SVS). Similar trends were also observed when ethanol was used as a processing solvent, but with slightly lower mobility. Ethanol-based FETs showed mobility of ≈0.3 $cm^2 V^{-1} s^{-1}$ under short channel device geometry, and mobility of ≈0.05 $cm^2 V^{-1} s^{-1}$ under long channel device geometry. According to the best of our knowledge, the obtained mobility values of 1.03 and 0.5 $cm^2 V^{-1} s^{-1}$ processed from butanol and ethanol are highest values in the field of PFETs processed with real "green" solvents and also clearly exceeds those of hydrogenated amorphous silicon semiconductors.[1] Additionally, we also fabricated low-voltage-operating PFETs using sol–gel processed ZrO_x as a dielectric layer, because low-voltage operation is another important criterion for industrial applications. The representative transfer curves obtained from the low-voltage operating regime are shown in Figure S9 of the Supporting Information. The obtained mobility reached as high as 0.5 $cm^2 V^{-1} s^{-1}$, implying that the alcohol-processing of P1 can also work for low power-consumption applications.

As confirmed by GIXD, the alcohol-processed P1 films have a relatively disordered crystalline nature, especially in terms of crystalline orientation. In the organic electronics field, the well-aligned and long-range-ordered microcrystalline structures of polymeric semiconductors have traditionally been believed to be a decisive factor to achieving efficient intermolecular interactions, and thus, high charge carrier mobility in PFETs.[32] However, recent studies have shown that this traditional rule may not necessarily be true in the case of highly conjugated donor-acceptor copolymers with planar backbone structure.[33,34] For example, Venkateshvaran et al. have revealed that a torsion-free, planar structure of a polymer backbone can be a more decisive factor for enhancing the charge transport characteristics of polymeric semiconductors, rather than the degree of crystallinity,[10] Our results—reasonably high mobility obtained from alcohol-processed P1 films—may also support the recent findings when considering the chemical structure of the P1 backbone: the thiophene unit attached to the DPP unit is known to lead to close (2.1 Å) intramolecular hydrogen bonding between the carbonyl oxygen of DPP and the nearest thiophene hydrogen that facilitates backbone planarity.[35] Therefore, we may argue that the highly planar nature of P1 enabled reasonably high charge carrier mobility, even when processed with alcohol, which leads to films consisting of noncontinuous, less-oriented micro-sized clusters. We believe that the alcohol-based polymer deposition technique described in this work can be fully utilized for all other low crystalline polymeric semiconductors with sufficient backbone planarity to ultimately realize environmentally benign and high-performance organic electronics.

3. Conclusion

Using a simple dispersion method of conjugated random copolymer in low-molecular-weight alcohols (ethanol, propanol, and butanol), we fabricated colloidal solutions of conjugated semiconducting polymer. Based on such sub-microparticles of semiconducting polymer, we have demonstrated high-performance ($\mu \approx 1.03$ $cm^2 V^{-1} s^{-1}$) PFETs from a "green" process. According to MSDSs and many other official resources, these alcohols are clearly more environmentally benign solvents than all other previously reported "relatively greener" solvents such as tetrahydronaphthalene or xylene. From various X-ray analyses, combined with FET measurements, we have proved that sub-microparticles of semiconducting polymer dispersed in alcohol still maintain crystalline order to some degree, which is enough to yield reasonably high mobility. Because this "green" deposition method simply utilizes physical aggregation of finely dispersed polymeric semiconductor clusters, it can be widely applied to other organic electronics fields.

4. Experimental Section

Materials: The synthetic procedure of P1—random copolymers consisting of diketopyrrolopyrrole-thienothiophene and diketopyrrolopyrrole-selenophene-vinylene-selenophene with composition ratios of 7:3—can be found from previous work.[19] PVDF ($M_w \approx 534\,000$), butanol, propanol, ethanol, butyraldehyde, and propionaldehyde were purchased from Sigma-Aldrich without further purification.

Characterization: Optical images of the transistors were obtained with a digital camera (Lumix DMC-LX5, Panasonic). SEM image was obtained by FE-SEM (Sigma/Carl Zeiss) with Schottky Field Emitter. The surface tension data were measured using tension meter (Kruss, K100). The XPS data of 50 um spatial resolutions were obtained from micro-area XPS scanning microscopy (Quantera II, ULVAC-PHI). The GIXD measurements were perfomed at PLS-II 9A U-SAXS beamline in conjunction with 4D beamline of Pohang Accelerator Laboratory (PAL) in Korea. The X-rays coming from the in-vacuum undulator (IVU) are monochromated (E = 11.06 keV) using Si(111) double crystals, were focused at the detector position using K-B focusing mirror system. The horizontal and vertical beam size is 300 (H) μm and 30 (V) μm, respectively. The incidence angle (α_i) was adjusted to 0.13° which was above the critical angle. GIXD patterns were recorded with a 2D CCD detector (Rayonix. SX-165). Diffraction angles were calibrated by a precalibrated sucrose (Monoclinic, P21) and the sample-to-detector distance was approximately 225 mm. The electrical characteristics of the transistors were measured by 4156A Precision semiconductor parameter analyzers (Agilent Technologies).

Fabrication: P1 and PVDF were dispersed in either ethanol or butanol (P1 2.5 mg/PVDF 2.5 mg in alcohol 1 mL) and sonicated for 2 to 6 h without further heating. Following sonication, the dispersion was stable up to 3 h before settling occurs. However, it was not the aggregation between particles and immediately well-dispersed by simple mechanical mixing. The aggregation happened after 4–5 d. Before spin-coating or drop-casting, minor amount of butyraldehyde or propionaldehyde (5 vol%) was added to the alcohol solution. The fabricated film was further annealed at hot-plate if requested. Au source-drain electrode was deposited onto either the polymer film or the Cr-treated Si wafer depending on the device structure. For sol–gel processed ZrO_x layer, a zirconium (IV) acetylacetonate ($Zr(acac)_4$) solution in *N*,*N*–dimethylformamide (DMF) at a 0.1 M concentration under a nitrogen atmosphere with the addition of equimolar ethanolamine was spin-coated by 4000 rpm for 30 s on a heavily doped Si wafer and cured under high temperature (400 °C) for 1 h in atmospheric condition.

Supporting Information

Supporting Information is available from the Wiley Online Library or from the author.

Acknowledgements

This research was supported by Space Core Technology Development Program through the National Research Foundation of Korea (NRF) funded by the Ministry of Education (Grant No. NRF-2014M1A3A3A02034707).

Received: March 5, 2015
Revised: June 8, 2015
Published online: July 2, 2015

[1] J. Li, Y. Zhao, H. S. Tan, Y. Guo, C.-A. Di, G. Yu, Y. Liu, M. Lin, S. H. Lim, Y. Zhou, H. Su, B. S. Ong, *Sci. Rep.* **2012**, *2*, 754.
[2] G. Kim, S.-J. Kang, G. K. Dutta, Y.-K. Han, T. J. Shin, Y.-Y. Noh, C. Yang, *J. Am. Chem. Soc.* **2014**, *136*, 9477.
[3] H.-R. Tseng, H. Phan, C. Luo, M. Wang, L. A. Perez, S. N. Patel, L. Ying, E. J. Kramer, T.-Q. Nguyen, G. C. Bazan, A. J. Heeger, *Adv. Mater.* **2014**, *26*, 2993.
[4] L. Derue, O. Dautel, A. Tournebize, M. Drees, H. Pan, S. Berthumeyrie, B. Pavageau, E. Cloutet, S. Chambon, L. Hirsch, A. Rivaton, P. Hudhomme, A. Facchetti, G. Wantz, *Adv. Mater.* **2014**, *26*, 5831.
[5] A. J. Barker, K. Chen, J. M. Hodgkiss, *J. Am. Chem. Soc.* **2014**, *136*, 12018.
[6] S. Park, B. T. Lim, B. Kim, H. J. Son, D. S. Chung, *Sci. Rep.* **2014**, *4*, 5482.
[7] S. K. Hwang, S.-Y. Min, I. Bae, S. M. Cho, K. L. Kim, T.-W. Lee, C. Park, *Small* **2014**, *10*, 1976.
[8] C. Luo, A. K. K. Kyaw, L. A. Perez, S. Patel, M. Wang, B. Grimm, G. C. Bazan, E. J. Kramer, A. J. Heeger, *Nano Lett.* **2014**, *14*, 2764.
[9] H. Sirringhaus, *Adv. Mater.* **2014**, *26*, 1319.
[10] D. Venkateshvaran, M. Nikolka, A. Sadhanala, V. Lemaur, M. Zelazny, M. Kepa, M. Hurhangee, A. J. Kronemeijer, V. Pecunia, I. Nasrallah, I. Romanov, K. Broch, I. McCulloch, D. Emin, Y. Olivier, J. Cornil, D. Beljonne, H. Sirringhaus, *Nature* **2014**, *515*, 384.
[11] W.-Y. Lee, G. Giri, Y. Diao, C. J. Tassone, J. R. Matthews, M. L. Sorensen, S. C. B. Mannsfeld, W.-C. Chen, H. H. Fong, J. B.-H. Tok, M. F. Toney, M. He, Z. Bao, *Adv. Funct. Mater.* **2014**, *24*, 3524.
[12] Z. B. Henson, P. Zalar, X. Chen, G. C. Welch, T.-Q. Nguyen, G. C. Bazan, *J. Mater. Chem. A.* **2013**, *1*, 11117.
[13] C. Xue, F.-T. Luo, H. Liu, *Macromolecules* **2007**, *40*, 6863.
[14] R. Cagnoli, M. Lanzi, E. Libertini, A. Mucci, L. Paganin, F. Parenti, L. Preti, L. Schenetti, *Macromolecules* **2008**, *41*, 3785.
[15] P. M. Beaujuge, C. M. Amb, J. R. Reynolds, *Adv. Mater.* **2010**, *22*, 5383.
[16] K. Lu, Y. Guo, Y. Liu, C.-a. Di, T. Li, Z. Wei, G. Yu, C. Du, S. Ye, *Macromolecules* **2009**, *42*, 3222.
[17] T. Kietzke, D. Neher, K. Landfester, R. Montenegro, R. Güntner, U. Scherf, *Nat. Mater.* **2003**, *2*, 408.
[18] H.-J. Yun, G. B. Lee, D. S. Chung, Y.-H. Kim, S.-K. Kwon, *Adv. Mater.* **2014**, *26*, 6612.
[19] H.-J. Yun, J. Cho, D. S. Chung, Y.-H. Kim, S.-K. Kwon, *Macromolecules* **2014**, *47*, 7030.
[20] All the MSDS data sheets were obtained from web-page of Sigma-Aldrich: www.sigmaaldrich.com (accessed: March 2015).
[21] R. K. Henderson, C. Jimenez-Gonzalez, D. J. C. Constable, S. R. Alston, G. G. A. Inglis, G. Fisher, J. Sherwood, S. P. Blinks, A. D. Curzons, *Green Chem.* **2011**, *13*, 854.
[22] E. S. Daniels, E. D. Sudol, M. S. El-Aasser, *Overview of Polymer Colloids: Preparation, Characterization, and Applications, ACS Symposium Series*, American Chemical Society, Washington **2002**.
[23] R. Lambourne, T. A. Strivens, *Paint and Surface Coatings – Theory and Practice*, 2nd ed., Woodhead Publishing Limited, Cambridge, England **1999**.
[24] J. Kreuter, R. N. Alyautin, D. A. Kharkevich, A. A. Ivanov, *Brain. Res.* **1995**, *674*, 171.
[25] H. J. Snaith, H. Kenrick, M. Chiesa, R. H. Friend, *Polymer* **2005**, *46*, 2573.
[26] Z. Li, A. N. Schwier, N. Sareen, V. F. Mcneill, *Atmos. Chem. Phys.* **2011**, *11*, 11617.
[27] The composition ratio was described in accordance with the feed ratio. Based on elemental analyses as shown in Table S6, we argue that the random copolymers studied in this paper can be assigned in accordance with their initial feed ratios.
[28] http://www.acs.org/gcipharmaroundtable (accessed: March 2015)
[29] J. Rivnay, S. C. B. Mannsfeld, C. E. Miller, A. Salleo, M. F. Toney, *Chem. Rev.* **2012**, *112*, 5488.
[30] A. M. Hindeleh, R. Hosemann, *J. Phys. C: Solid State Phys.* **1988**, *21*, 4155.
[31] M. R. Hammond, R. J. Kline, A. A. Herzing, L. J. Richter, D. S. Germack, H.-W. Ro, C. L. Soles, D. A. Fischer, T. Xu, L. Yu, M. F. Toney, D. M. DeLongchamp, *ACS Nano* **2011**, *5*, 8248.
[32] I. McCulloch, M. Heeney, C. Bailey, K. Genevicius, I. MacDonald, M. Shkunov, D. Sparrowe, S. Tierney, R. Wagner, W. Zhang, M. L. Chabinyc, R. J. Kline, M. D. Mcgehee, M. F. Toney, *Nat. Mater.* **2006**, *5*, 328.
[33] X. Zhang, H. Bronstein, A. J. Kronemeijer, J. Smith, Y. Kim, R. J. Kline, L. J. Richter, T. D. Anthopoulos, H. Sirringhaus, K. Song, M. Heeney, W. Zhang, I. McCulloch, D. M. Delongchamp, *Nat. Commun.* **2013**, *4*, 2238.
[34] R. Noriega, J. Rivnay, K. Vandewal, F. P. V. Koch, N. Stingelin, P. Smith, M. F. Toney, A. Salleo, *Nat. Mater.* **2013**, *12*, 1038.
[35] P.-T. Wu, F. S. Kim, S. A. Jenekhe, *Chem. Mater.* **2011**, *23*, 4618.